Structures and Stabilities of Fe2+/3+ Complexes Relevant to Alzheimer's Disease: An ab Initio Study

ARTICLE *in* THE JOURNAL OF PHYSICAL CHEMISTRY A · JUNE 2011

Impact Factor: 2.69 · DOI: 10.1021/jp2026626 · Source: PubMed

4 AUTHORS:

Jorge Alí-Torres
National University of Colombia
25 PUBLICATIONS **124** CITATIONS
SEE PROFILE

Luis Rodríguez-Santiago
Autonomous University of Barcelona
73 PUBLICATIONS **1,671** CITATIONS
SEE PROFILE

Mariona Sodupe
Autonomous University of Barcelona
189 PUBLICATIONS **4,600** CITATIONS
SEE PROFILE

Arvi Rauk
The University of Calgary
245 PUBLICATIONS **8,149** CITATIONS
SEE PROFILE

THE JOURNAL OF PHYSICAL CHEMISTRY A

ARTICLE

pubs.acs.org/JPCA

Structures and Stabilities of $Fe^{2+/3+}$ Complexes Relevant to Alzheimer's Disease: An ab Initio Study

Jorge Alí-Torres,[†] Luis Rodríguez-Santiago,[†] Mariona Sodupe,[†] and Arvi Rauk*[,‡]

[†]Departament de Química, Universitat Autònoma de Barcelona, Bellaterra 08193, Spain

[‡]Department of Chemistry, University of Calgary, Calgary AB, T2N 1N4, Canada

Supporting Information

ABSTRACT: Iron is one of the most abundant metals found in senile plaques of post mortem patients with Alzheimer's disease. However, the interaction mode between iron ions and β-amyloid peptide as well as their precise affinity is unknown. In this study we apply ab initio computational methodology to calculate binding energies of $Fe^{2+/3+}$ with the His13-His14 sequence of Aβ, as well as other important ligands such as His6 and Tyr10. Calculations were carried out at the "MP2/6-311+G(2df,2p)"//B3LYP/6-31+G(d) level of theory and solvent effects included by the IEFPCM procedure. Several reaction paths for the binding of imidazole, phenol, and the His13-His14 fragment (modeled by *N*-(2-(1*H*-imidazol-4-yl)ethyl)-3-(1*H*-imidazol-4-yl)propanamide) were sequentially explored. The results show that the most stable complexes containing His13-His14 and phenolate of Tyr10 are the pentacoordinated $[Fe^{2+}(O\text{-HisHis})(PhO^-)(H_2O)]^+$ and $[Fe^{3+}(N\text{-HisHis})(PhO^-)(H_2O)]^+$ compounds and that simultaneous coordination of tyrosine and His13-His14 to $Fe^{2+/3+}$ is thermodynamically favorable in water at physiological pH. Computed Raman spectra confirm the conclusion obtained by Miura et al. (Biochemistry 2000, 39, 7024) that tyrosine is coordinated to Fe^{3+} but do not exclude coordination of imidazoles. Finally, calculations of standard reduction potentials indicate that phenol coordination reduces the redox activity of the iron/Aβ complexes.

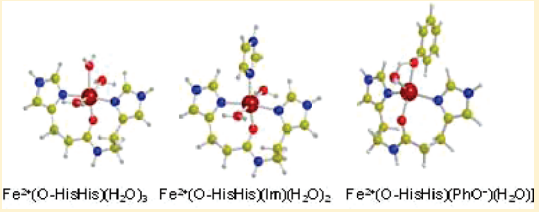

INTRODUCTION

Alzheimer's disease (AD) is the most common form of neurodegenerative dementia. It is caused by an aggregated form of the amyloid β-peptide (Aβ) that induces massive loss of brain cells due to brain inflammation and membrane destruction.[1,2] Aβ is a polypeptide of variable length, from 39 to 43 residues. The two main isoforms are Aβ1−40 and Aβ1−42, which have the following sequence in single-letter code:

$D_1AGFRH_6DSGY_{10}EVH_{13}H_{14}QKLVFFAEDVGSNKGAII-GLMVGGVVIA_{42}$

It is well-known that some biologically available metals, such as copper, zinc, and iron, interact with Aβ.[3] Research into the roles of metal ions has been hampered by the fact that neither Aβ itself nor any of its complexes with metal ions form crystals that can be analyzed by X-ray diffraction experiments. In this context high-level computational modeling can provide useful structural information as well as considerable insight into the damaging mechanisms of the Aβ/metal complexes.

The role of copper and zinc ions has been studied extensively.[2−10] The coordination environment of Cu^{2+} in soluble Cu^{2+}-Aβ complexes seems to be highly sensitive to the pH, and experimental data suggest that several distinct modes can coexist. The most likely structures imply a square-planar configuration of Cu^{2+} coordinated to the three N atoms of His residues while the fourth ligand could be an oxygen atom or the N-terminus group.[2] However, iron, one of the most abundant metals in the body, which may be highly redox active and is found in senile plaques of post mortem AD patients,[11] has not been extensively studied either experimentally or theoretically in the context of Aβ and Alzheimer's disease. Aβ is not believed to have a high affinity for iron ions, Fe^{2+} and Fe^{3+}, but the precise affinity is not known. Work by Miura et al.[12] using Raman spectroscopy to study Fe^{3+}-Aβ complexes, showed that iron binds Aβ via the phenolic oxygen of Tyr10. On the other hand, this study suggests that histidines in the N-terminal hydrophilic region of Aβ do not bind to Fe^{3+}.[13] In contrast, Nakamura et al.[14] state that His6, His13 and His 14 residues control the redox activity of the transition metal present in the senile plaques based on a study of the redox behavior of Cu^{2+} and Fe^{3+} in the presence of Aβ. The relevance of the study of Fe-Aβ interaction arises from the possible ability of this metal to promote the Fenton reaction generating reactive oxygen species (ROS), another important hallmark in AD.[15]

The involvement of iron ions in AD pathology constitutes a possible important new avenue of research into the mechanism of AD. For this reason, more information about iron-Aβ interactions is needed to understand the nature and properties of these complexes. In this study we apply ab initio computational methodology to calculate binding energies of $Fe^{2+/3+}$ with the His13-His14 sequence, which binds copper and raises its reduction potential,[9] as well as other important ligands such as His6

Special Issue: Richard F. W. Bader Festschrift

Received: March 21, 2011
Revised: May 9, 2011
Published: June 16, 2011

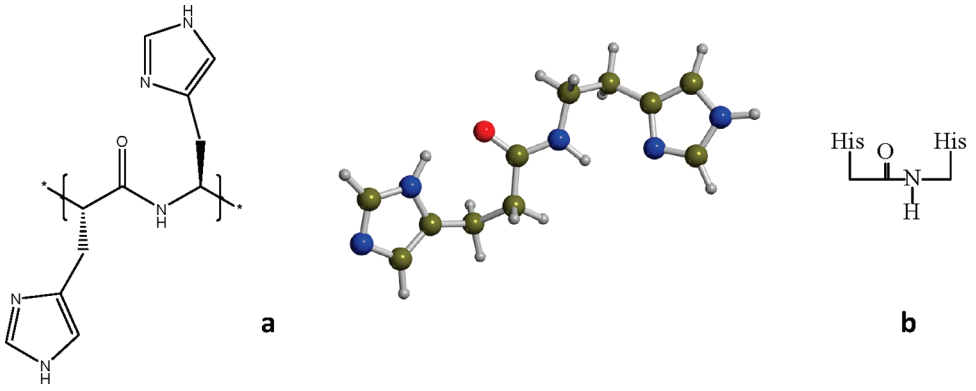

Figure 1. (a) *N*-(2-(1*H*-imidazol-4-yl)ethyl)-3-(1*H*-imidazol-4-yl)propanamide as model for the His13-His14 sequence of Aβ. (b) Schematic representation used in this work for simplicity.

and Tyr10. The main goal of this work is to determine whether or not the histidines and tyrosine of human Aβ can bind to $Fe^{2+/3+}$ and estimate their affinity constants and redox activity. Moreover, the Raman spectra of the most stable iron complexes are computed and compared to the experimental data.[13] Results show that coordination to histidine imidazoles and to the phenol ring from tyrosine is plausible and that the computed Raman spectra of the most stable structures are in accordance with those obtained in the Raman spectroscopy study of Miura et al.,[12] which provides evidence for this kind of coordination.

COMPUTATIONAL METHODS

Density functional theory (DFT) calculations were carried out using the Gaussian 03[16] and Gaussian 09[17] suite of programs. Geometry optimizations and vibrational frequency analysis were performed using the Becke three-parameter hybrid functional (B3LYP) method[18−20] with the small basis set, SB (SB = 6-31+G(d)). A scale factor of 0.9806[21] was used to scale the zero-point energies. Unscaled frequencies were used to derive entropies and thermal corrections to the enthalpy. A term $R\ln(n)$ was added to the entropy of each species, where n was an estimate (based on simple rotamer counting) of the number of significantly populated conformers.[22] This term is required to take into account changes in the gain or loss of entropy due to breaking or making cyclic structures. To obtain more accurate energy changes, and to determine the effect of increasing the basis set, single-point calculations at the optimized geometries with the SB basis set were carried out at the B3LYP level with the larger basis set, LB (LB = 6-311+G(2df,2p)). B3LYP has been found to perform satisfactorily for predicting the spin states of iron complexes.[23] We studied four-, five-, and six-coordinate iron complexes. For Fe^{2+} complexes, the singlet, triplet, and quintet states were considered, while for Fe^{3+} complexes, the doublet, quartet, and sextet spin states were investigated. All the calculations were carried out using the spin-unrestricted formalism for open shell systems. In all cases high spin states were found to be the lowest ones with B3LYP. Moreover, MP2 calculations were carried out for some systems, and in all cases the trends observed on the relative energies for the different spin multiplicities were in accordance with the B3LYP ones (Table S2 of the Supporting Information (SI)).

For all of the systems, single point calculations were also carried out at the MP2/SB level on the B3LYP/SB geometries of the lowest energy spin states. It was not feasible to carry out MP2/LB calculations for most of the systems of interest here. Thus, the MP2 energies, adjusted for basis set size by the additive approximation, $E(\mathrm{MP2/LB}) \approx E(\mathrm{MP2/SB}) + E(\mathrm{B3LYP/LB}) - E(\mathrm{B3LYP/SB})$, were used as alternatives to the B3LYP/LB energies to calculate binding affinities. The B3LYP/SB wave function was used as the "guess" for the UHF/SB calculation that precedes the UMP2 procedure. The reliability of this approximation was confirmed by performing MP2/LB calculations for some selected systems (Table S8 of SI). The computed reaction energies by using estimated or exact MP2/LB values differ by $\approx$5 kJ mol^{-1}, being systematically more exergonic when exact values are used.

The polarizable continuum model (PCM) using the integral equation formalism variant (IEFPCM)[24] was used to calculate the free energy of solvation in water. UAHF default scaled radii were used to define the solvent cavities.[25] Experimental free energies of solvation were used for H_2O (ΔG_{solv} = −26.4 kJ mol^{-1})[26] and H^+ (ΔG_{solv} = −1107 kJ mol^{-1}).[27] An addition of 10 kJ mol^{-1} ($RT\ln(55.6)$) was made to the free energy of solvation of water, because liquid water concentration is 55.6 M.

Standard reduction potentials, $E°(\text{"}Fe^{3+}\text{"}/\text{"}Fe^{2+}\text{"})$ vs the standard hydrogen electrode (SHE), were calculated from the half reactions,

$$\text{"}Fe^{3+}\text{"}_{(aq)} + e^- \rightarrow \text{"}Fe^{2+}\text{"}_{(aq)} + aL \qquad \Delta G^{Fe}$$

and

$$H^+ + e^- \rightarrow 1/2H_2 \qquad \Delta G^{SHE}$$

where "Fe^{3+}" and "Fe^{2+}" represent all of the oxidized and reduced iron species involved in the reduction, and ΔG^{Fe} and ΔG^{SHE} are the aqueous free energy changes for the respective half reactions, ignoring the electron. The symbol aL recognizes the fact that a number of ligands may be shed in the reduction process, and the associated entropy change may be an important component of the free energy change. Thus,

$$E°(\text{"}Fe^{3+}\text{"}/\text{"}Fe^{2+}\text{"}) = -(\Delta G^{Fe} - \Delta G^{SHE})/F$$

where F is the Faraday constant, F = 96.485 kJ mol^{-1} V^{-1}. For the reduction of the proton, we adopt the experimental value, ΔG^{SHE} = −418 kJ mol^{-1}.[28] The actual potential, E, of the half reaction under ambient conditions is related to the standard potential, $E°$, through Nernst equation:

$$E = E° - (RT/F)\ln Q$$

where Q is the reaction quotient specifying concentrations of oxidized and reduced components and other species associated

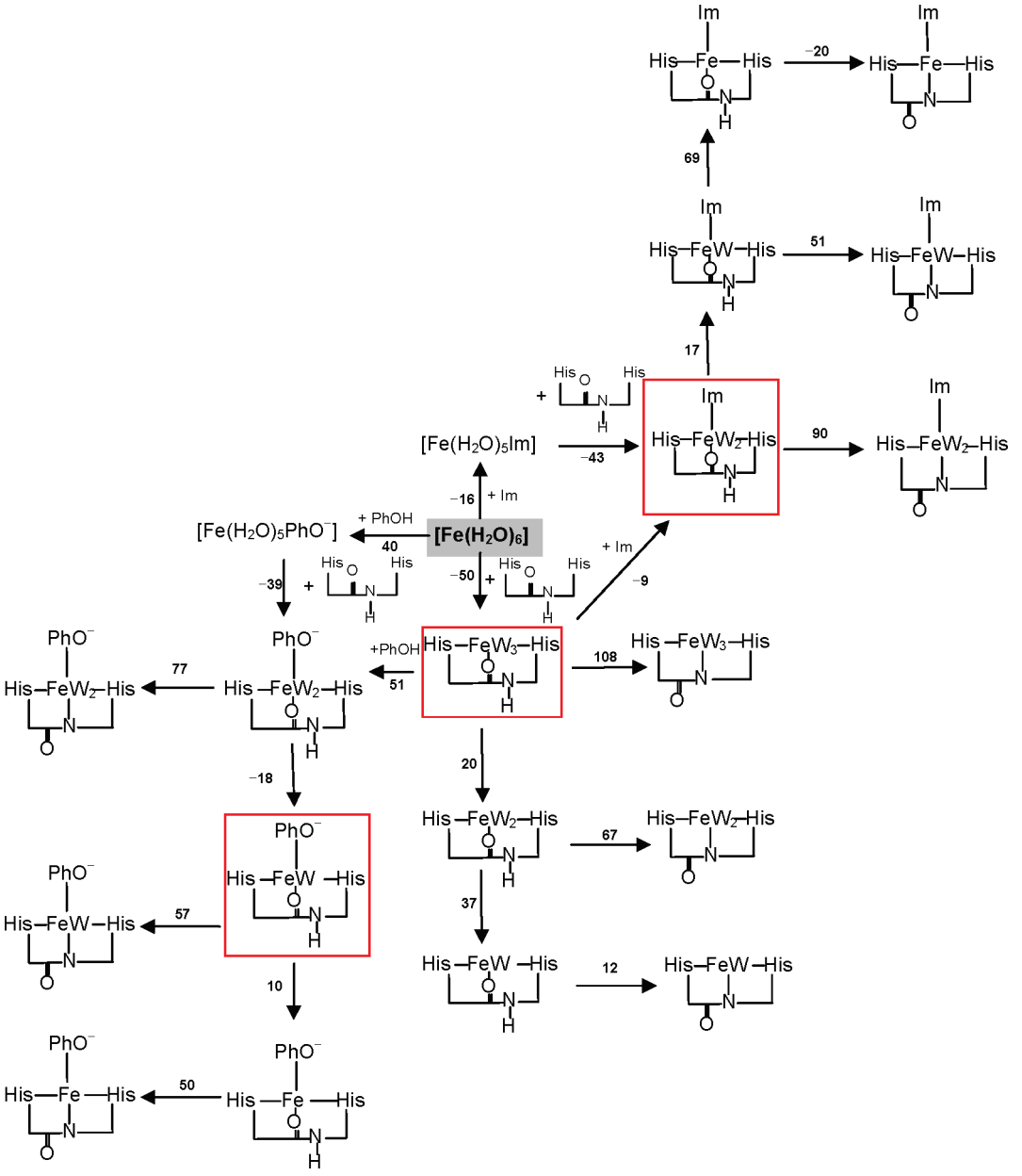

Figure 2. Binding path showing ΔG_{aq} in kJ mol^{-1} for Fe^{2+} complexes. When ΔG_{aq} is pH-dependent, the value at pH = 7 is presented. Water molecules (represented as W) and protons are not shown when released in a reaction. Most stable models are highlighted in boxes and starting complex in bold.

with the chemical change. In the special case that n protons are consumed in solution buffered at pH 7 under otherwise standard conditions, the reaction quotient reduces to $Q = 10^{7n}$, and the symbol $E^{o\prime} = E^{\circ} - (RT/F) \ln Q = E^{\circ} - 0.41n$ V).[9]

RESULTS AND DISCUSSION

The optimized geometries and calculated data for all the species studied in this work are presented in Table S1−S9 (SI). Tables S4 and S5 (SI) show the reaction energies of Fe^{2+} and Fe^{3+} complexes with the aforementioned ligands and the subsequent water dissociation and deprotonation reactions at the MP2 level of theory. Tables S6 and S7 (SI) show the equivalent values of Fe^{2+} and Fe^{3+} complexes at the B3LYP level, respectively. The differences between "MP2/LB" and B3LYP/LB values are smaller than 52 kJ mol^{-1} for Fe^{2+} complexes. For Fe^{3+} complexes, the differences are larger, up to 132 kJ mol^{-1}, for some particular cases. Although major trends on the stability of the different systems are preserved with both methods, the results reveal that B3LYP tends to favor less coordinated complexes (Tables S4−S7 of SI). On the other hand, previous results on similar iron containing complexes have shown that the "MP2/LB" approximation provides values in very good agreement with the experimental results.[29] For this reason, hereafter, all the Results and Discussion will refer to "MP2/LB"-derived data. As mentioned, the main goal of this work is to determine whether or not histidines and tyrosine of human Aβ can bind to $Fe^{2+/3+}$ as well as to estimate their affinity constants. We focus mainly on the binding of $Fe^{2+/3+}$ to the His13-His14 region of Aβ, which was modeled by *N*-(2-(1*H*-imidazol-4-yl)ethyl)-3-(1*H*-imidazol-4-yl)propanamide (Figure 1). His6 was modeled by an imidazole and Tyr10 by a phenol group. It should be noted that in the present work, His13-His14 coordination has been

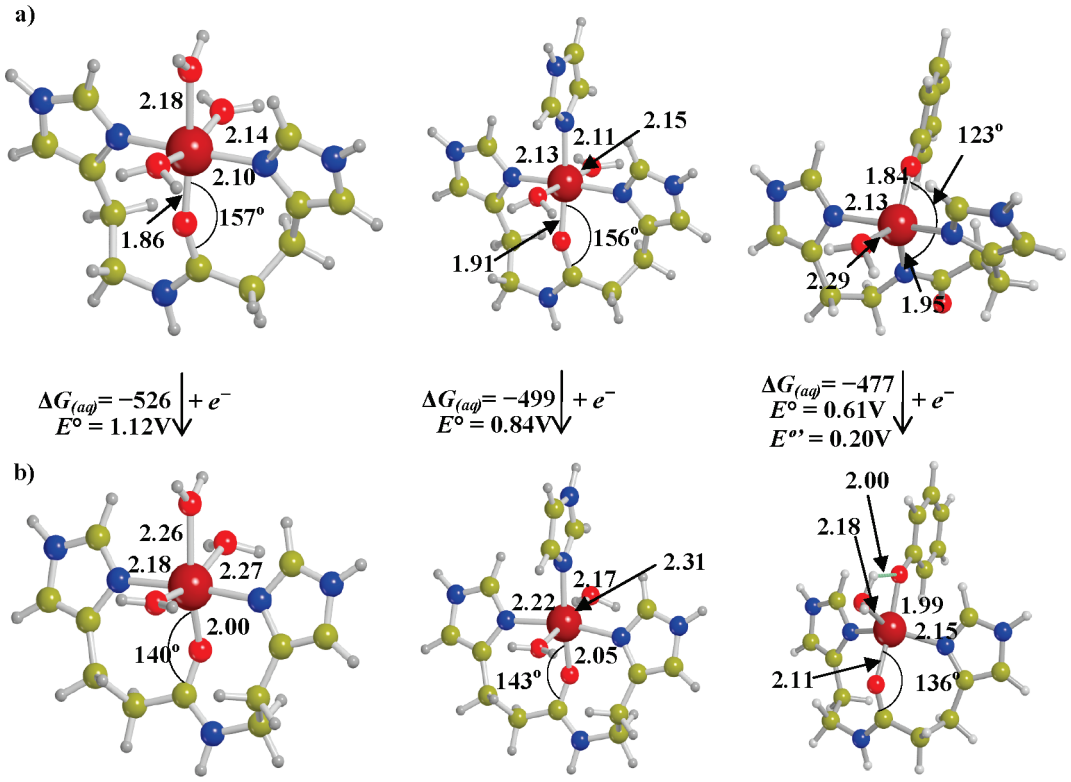

Figure 3. B3LYP/6-31+G(d) optimized geometries for most stable models of (a) Fe^{3+} and (b) Fe^{2+} complexes. Bond lengths are expressed in angstroms and angles in degrees. Standard reduction potentials vs standard hydrogen electrode and aqueous free energies (kJ mol^{-1}) are also shown.

assumed to occur through the N_δ of the imidazoles, facilitating the interaction of the peptide backbone, because previous theoretical work with the Cu^{2+} complexes have shown that is the preferred mode of coordination.[7]

Fe^{2+} Coordination to His13-His14 Sequence, His6 and Tyr. The reaction energies associated with His13-His14 sequence, His6 and Tyr coordination to Fe^{2+}, and the reaction paths are summarized in Figure 2. The reference structure is the hexaaquo iron complex, $[Fe^{2+}(H_2O)_6]^{2+}$. The substitution of one water molecule by imidazole is exergonic (ΔG_{aq}= −16 kJ mol^{-1}) whereas substitution by phenol is endergonic (ΔG_{aq}= 40 kJ mol^{-1}) at pH = 7. The calculated affinity constants (calculated as $K_{aff} = e^{-\Delta G/RT}$) are 6.4 × 10^2 and 9.7 × 10^{-8}, respectively. To calculate the free energies for all the reactions where a proton is involved, we added the term RT ln Q, where Q is the reaction quotient, which simplifies to $[H^+]$ as all other relevant species are 1 M at pH 7. This term needs to be added to the free energy change because the pK_a of phenol is larger than 7 and thus, at this pH the protonated form would be present in >99% abundance.[30] For the coordination of the His13-His14 fragment we considered two possibilities: (i) coordination through N_δ of imidazoles and the oxygen from the backbone (O_C), hereafter referred to *O*-His-His (e.g., $[Fe^{2+}(O\text{-HisHis})(H_2O)_3]^{2+}$) and (ii) coordination involving the same nitrogen atoms from imidazoles and the N from the backbone, referred to *N*-His-His. Note that this latter coordination implies a deprotonation of the backbone. The calculations indicate that the coordination of the peptide fragment is more favorable through the O atom than through the N one. The optimized structure of this complex is given in Figure 3 and shows short bond distances as well as very low Jahn−Teller effect in the axial water molecules, as expected for d^6 high spin complexes. The aqueous free energy of binding for His-His is highly exergonic (ΔG_{aq} = −50 kJ mol^{-1}). The computed affinity constant (K_{aff} = 6.3 × 10^8) is higher than that calculated at the same level of theory for the corresponding Cu^{2+} complex, K_{aff} = 2.0 × 10^6.[31] Values reported experimentally for CuAβ(1−40) and N-terminal fragments vary from 10^5 to 10^{10},[32] with a preference for the higher value,[4] although a very high value, K_{aff} = 1.6 × 10^{17}, has been reported for CuAβ(1−42).[33] The deprotonation and coordination through the N atom of the backbone is unfavorable for all the possible complexes considered here. Thus, $[Fe^{2+}(O\text{-HisHis})(H_2O)_3]^{2+}$ is the most stable complex for the single substitution of the His13-His14 fragment.

Starting from $[Fe^{2+}(O\text{-HisHis})(H_2O)_3]^{2+}$, we studied the substitution of one water molecule by either imidazole or phenol. The optimized geometries of these complexes are shown in Figure 3. Computed reaction energies indicate that the water displacement by imidazole is slightly exergonic (ΔG_{aq} = −9 kJ mol^{-1}, K_{aff} = 37.8), which corresponds to a global aqueous free energy change of ΔG_{aq}= −59 kJ mol^{-1} if the hexaaquo iron complex is considered as the initial complex. Interestingly, the results show that the displacement reaction involving the His13-His14 fragment is more than 3 times more exergonic than with the third imidazole, starting from the hexaaquo iron complex, which points out the effect of chelation and the importance of peptide coordination through the carbonyl oxygen. Water dissociation and deprotonation from this complex is unfavorable. Thus, $[Fe^{2+}(O\text{-HisHis})(Im)(H_2O)_2]^{2+}$ is the most stable complex enclosing both the His-His fragment and imidazole.

The substitution of one water molecule by a phenol group in $[Fe^{2+}(O\text{-HisHis})(H_2O)_3]^{2+}$ is, however, unlikely. The aqueous free energy change for this reaction is 51 kJ mol^{-1} at pH = 7, which

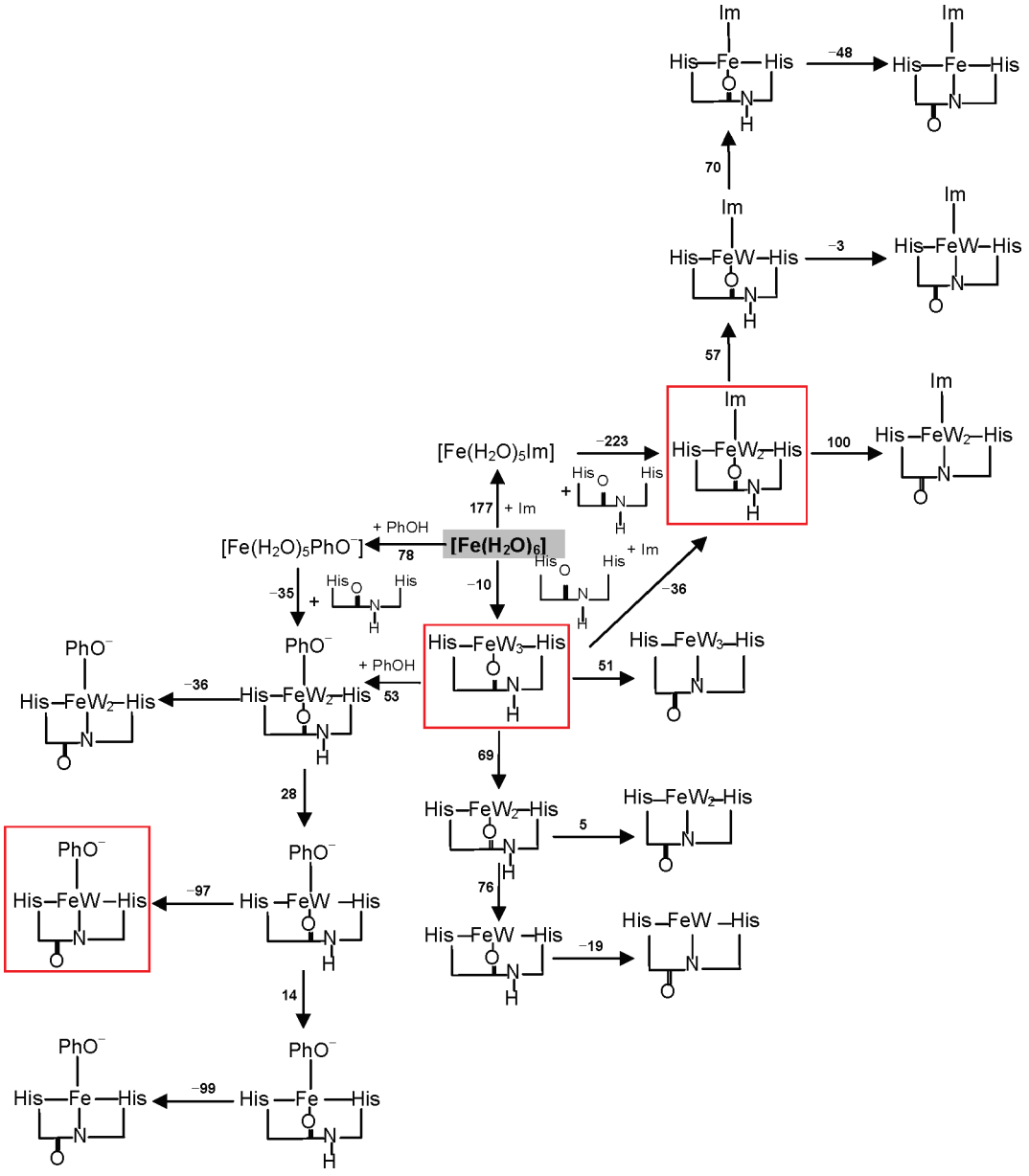

Figure 4. Binding path showing ΔG_{aq} in kJ mol^{-1} for Fe^{3+} complexes. When ΔG_{aq} is pH-dependent the value at pH = 7 is presented. Water molecules (represented as W) and protons are not shown when released in a reaction. Most stable models are highlighted in boxes and starting complex in bold.

corresponds to a calculated affinity constant of $K_{aff} = 1.2 \times 10^{-9}$ (Figure 2). In contrast with the imidazole complex, the dissociation of one water molecule from this complex is exergonic by −18 kJ mol^{-1}; hence the global reaction up to this point, considering the hexaaquo ion as starting complex, is favorable by −17 kJ mol^{-1}. The deprotonation of the NH from the backbone and the dissociation of additional water molecules are thermodynamically unfavorable processes. As a result, $[Fe^{2+}(O\text{-HisHis})(PhO^-)(H_2O)]^+$ is the most stable complex that contains the His-His and PhO^- ligands. The optimized geometry of this complex is also shown in Figure 3. Remarkably, the axial coordinated water molecule establishes an H-bond interaction with the phenolic oxygen atom.

Fe^{3+} Coordination to His13-His14 Sequence, His 6 and Tyr. The corresponding reactions for Fe^{3+} and reactions paths are represented in Figure 4. The first remarkable observation is that the reaction free energies for the single ligand (imidazole and phenol) substitution are strongly endergonic, ΔG_{aq}= 177 kJ mol^{-1} and ΔG_{aq}= 78 kJ mol^{-1} respectively, largely due to highly unfavorable loss of free energy of solvation (Table S5 in SI). However, the coordination of the dipeptide His13-His14 is favorable, but only by −10 kJ mol^{-1}, which again highlights the importance of the peptidic bond and the effect of chelation in the coordination. Note that there is a strong interaction between Fe^{3+} and O_C, evidenced by a short bond distance of 1.86 Å (Figure 3). The subsequent water dissociations and the deprotonation of the N from the backbone are energetically unfavorable, and thus, the most stable structure corresponds to that with three water molecules in its coordination sphere, $[Fe^{3+}(O\text{-HisHis})(H_2O)_3]^{3+}$. Geometrically, it can be observed in Figure 3 that, as expected, the metal−ligand bond distances are shorter than in Fe^{2+} complexes, due to an enhanced electrostatic interaction.

dx.doi.org/10.1021/jp2026626 |J. Phys. Chem. A 2011, 115, 12523–12530

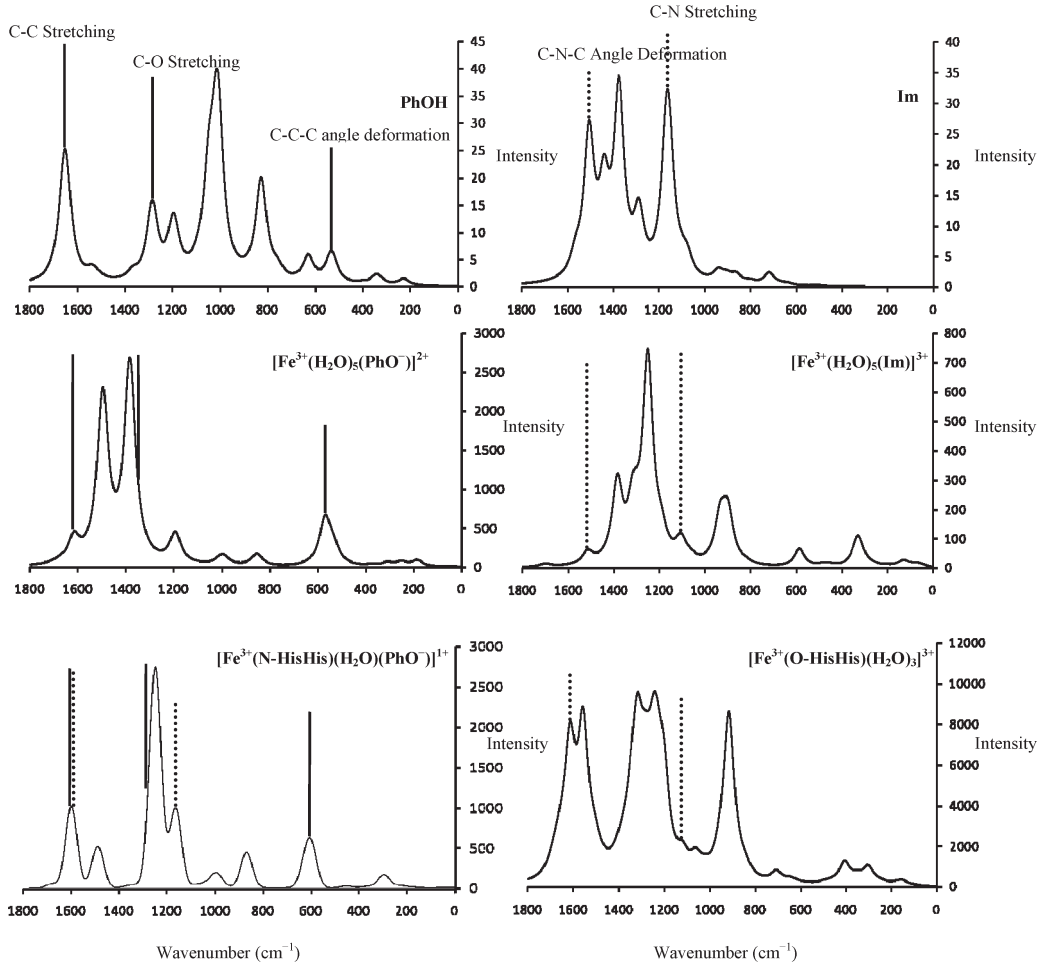

Figure 5. Raman spectra for the most stable Fe^{3+} complexes with the considered ligands. Dotted lines correspond to signals due to imidazole vibrations and solid lines are related to phenol group contributions. Note different scales are used in the intensity axis for each spectrum.

Considering $[Fe^{3+}(O\text{-HisHis})(H_2O)_3]^{3+}$ as the starting point, and similarly to the Fe^{2+} case, we studied the displacement reaction of one water molecule by imidazole and phenol. The reaction with imidazole is exergonic by −36 kJ mol^{-1} and, thus, more favorable than the analogous one involving the hexaaquo iron complex. This aqueous free energy change corresponds to an affinity constant of 2.0×10^6. The global reaction starting from the hexaaquo iron is favorable by −46 kJ mol^{-1}. Additional water dissociations and deprotonations are unlikely in this context. On the other hand, the reaction involving a phenol is endergonic by 53 kJ mol^{-1}. Although the second water dissociation is still endergonic, N−H deprotonation of the formed complex, $[Fe^{3+}(O\text{-HisHis})(PhO^-)(H_2O)]^{2+}$, yielding $[Fe^{3+}(N\text{-HisHis})(PhO^-)(H_2O)]^{+}$, is strongly exergonic (ΔG_{aq}= −97 kJ mol^{-1}). Indeed, deprotonation processes in Fe^{3+} complexes are much more favorable than in the Fe^{2+} ones. This is mainly due to the larger positive charge in the former, which produces a larger increase of the NH acidity. Consequently, the overall formation of $[Fe^{3+}(N\text{-HisHis})(PhO^-)(H_2O)]^{+}$ is favorable by −26 kJ mol^{-1} from $[Fe^{3+}(H_2O)_6]^{3+}$.

Extrapolating the above results to the case of Aβ, aqueous Fe^{3+} can bind initially to the His13-His14 region to form the complex (modeled by $[Fe^{3+}(O\text{-HisHis})(H_2O)_3]^{3+}$), and subsequently add a third His (e.g., His6). Addition of Tyr10 can proceed through a high energy intermediate that deprotonates and rearranges to the amide backbone N-coordinated complex, modeled by $[Fe^{3+}(N\text{-HisHis})(PhO^-)(H_2O)]^{+}$. The overall reactions to form the two complexes from aqueous Fe^{3+} and Aβ are both exergonic at physiological pH (−26 kJ mol^{-1} for $[Fe^{3+}(N\text{-HisHis})(PhO^-)(H_2O)]^{+}$ and −46 kJ mol^{-1} for $[Fe^{3+}(O\text{-HisHis})(Im)(H_2O)_2]^{3+}$). In the present study, we do not analyze the kinetic factors, which may also influence the formation of these stable compounds. The simultaneous coordination of both imidazole and phenolic ligands is, however, plausible on energetic grounds, which is further supported by comparison of calculated Raman spectra with the experimental spectra of Miura et al.,[12] discussed below.

Raman Spectra for Most Stable Fe^{3+} Models. Raman spectra for the most stable complexes of Fe^{3+} containing the phenolate group, representing tyrosine, and imidazole, representing histidine, were calculated using harmonic normal vibrational modes scaled by a factor of 0.9806.[21] The most relevant spectra are shown in Figure 5, and the values of the most significant frequencies of each system are summarized in Table S8 of the SI. To analyze the influence of coordination to Fe^{3+}, we first simulated the Raman spectra of free phenol and imidazole and selected some specific vibrations in the fingerprint region to compare. For phenol, we selected the C−C stretching, the C−O stretching, and the C−C−C angle deformation, which occur in the range 500 to 1700 cm^{-1}. The Raman spectrum for the $[Fe^{3+}(H_2O)_5(PhO^-)]^{2+}$ complex shows an important increase

dx.doi.org/10.1021/jp2026626 |J. Phys. Chem. A 2011, 115, 12523–12530

in the intensity of those signals. The observed shifts upon coordination are, however, small. As expected, the largest increase in intensity is predicted for the C−O stretching, due to the Fe^{3+}−O interaction, in agreement with that found experimentally by Miura et al.[12]

For imidazole, the C−N stretching and C−N−C angle deformation vibrations were selected as references. In these cases we also observed an important increase in the intensity of these signals in the imidazole containing complexes: $[Fe^{3+}(H_2O)_5(Im)]^{3+}$ and $[Fe^{3+}(O\text{-HisHis})(H_2O)_3]^{3+}$, as compared to free imidazole and small shifts upon metal coordination. Interestingly, imidazole C−N−C bending peak shifts from being ∼60 cm^{-1} lower than the C−C stretching peak of phenol in the spectra of the free ligands (PhOH and Im in Figure 5) to appear almost at the same frequency in the spectrum of the $[Fe^{3+}(N\text{-HisHis})(H_2O)(PhO^-)]^+$ complex (Figure 5). Thus, the band at ∼1600 cm^{-1} in the Raman spectrum of $[Fe^{3+}(N\text{-HisHis})(H_2O)(PhO^-)]^+$, containing both phenolate and imidazole ligands, may arise from the overlap of both vibrational modes. This possibility was not considered by Miura et al. in their experimental work, where the band at 1604 cm^{-1} was assigned to the tyrosinate. On the basis of our calculations, we conclude that the coordination of imidazole cannot be excluded, as suggested in the experimental study. Furthermore, according to the reaction energies previously discussed, the formation of a Fe^{3+} complex including both imidazole and phenolate is perfectly possible.

Reduction Behavior of the Iron Complexes. Because $Fe^{3+/2+}$ complexes have been suggested to be involved in the Fenton reaction, we have computationally determined the influence of His-His and Tyr coordination on the reduction potential of the Fe^{3+}/Fe^{2+} couple. The experimental value of the standard reduction potential for the Fe^{3+}/Fe^{2+} couple is 0.77 V.[34] In our simulation we obtained an aqueous free energy of −486 kJ mol^{-1} for the half-reaction from $[Fe^{3+}(H_2O)_6]^{3+}$ to $[Fe^{2+}(H_2O)_6]^{2+}$, which corresponds to a reduction potential of 0.70 V (vs the SHE). The computed standard reduction potential ($E°$) and the involved species are given in Figure 3. The coordination of the His13-His14 fragment is predicted to increase $E°$ to 1.12 V, while the successive coordination of the third imidazole and phenol group decreases this value to 0.84 and 0.61 V, respectively. Furthermore, the reduction of the $[Fe^{3+}(N\text{-HisHis})(PhO^-)(H_2O)]^+$ to $[Fe^{2+}(O\text{-HisHis})(PhO^-)(H_2O)]^+$ complex implies a reprotonation of the backbone. Thus, at pH = 7, $E°' = 0.20$ V.

CONCLUSIONS

The binding of Tyr and His-His fragment to $Fe^{2+/3+}$ complexes was investigated at the "MP2/6-311+G(2df,2p)"//B3LYP/6-31+G(d) level of theory and included solvent effects by the IEFPCM procedure. Several possible paths for the binding of imidazole, phenol, and HisHis fragment (modeled by *N*-(2-(1*H*-imidazol-4-yl)ethyl)-3-(1*H*-imidazol-4-yl)propanamide) were sequentially explored. Both for Fe^{2+} and for Fe^{3+} metal ions, the most stable complexes containing the His-His fragment and imidazole are the hexacoordinated $[Fe^{2+/3+}(O\text{-HisHis})(Im)(H_2O)_3]^{2+/3+}$ compounds in which the peptide bond interacts with the metal ion through the carbonyl oxygen. However, the most stable complexes containing His-His and phenolate are the pentacoordinated $[Fe^{2+}(O\text{-HisHis})(PhO^-)(H_2O)]^+$ and $[Fe^{3+}(N\text{-HisHis})(PhO^-)(H_2O)]^+$ compounds. Computed reaction energies indicate that simultaneous coordination of tyrosine and His13-His14 to Fe^{2+} and Fe^{3+} is thermodynamically favorable. Raman spectra for the most stable models confirm the conclusion obtained by Miura et al.[12] that tyrosine is coordinated to Fe^{3+}. However, the predicted changes in Raman intensities for $[Fe^{3+}(N\text{-HisHis})(PhO^-)(H_2O)]^+$ (compared to uncomplexed imidazole and phenol), as well as the fact that some phenol and imidazole signals overlap, do not exclude the HisHis group of Aβ as a possible ligand. Finally, calculations of standard reduction potentials of the model Fe/Aβ complexes indicate that Tyr coordination reduces the $Fe^{3+/2+}$ reduction by about 0.5 V compared to aqueous $Fe^{3+/2+}$ under physiological conditions.

ASSOCIATED CONTENT

Supporting Information. Tables showing the Cartesian coordinates of all species, relative energies for the different spin multiplicities, primary calculated data for B3LYP/6-31+G(d) and B3LYP/6-311+G(2df,2p) energies, zero-point and thermal corrections, free energies of solvation in water, and MP2/6-31+G(d) energies, detailed aqueous reaction energies for both "MP2/LB" and B3LYP/LB level of theories, and Raman frequencies. This material is available free of charge via the Internet at http://pubs.acs.org.

ACKNOWLEDGMENT

J.A-T. acknowledges the Spanish Ministry of Science and Innovation for the provision of the graduate studentship BES-2007-14304. This work was supported by the Natural Sciences and Engineering Council of Canada (NSERC) and by the Spanish Ministry of Science and Innovation (MICINN) through project CTQ2008-06381. We thank WestGrid for generous allocations of computational resources.

REFERENCES

(1) Rauk, A. *Dalton Trans.* **2008**, 1273.
(2) Rauk, A. *Chem. Soc. Rev.* **2009**, *38*, 2698.
(3) Hung, Y. H.; Bush, A. I.; Cherny, R. A. *J. Biol. Inorg. Chem.* **2010**, *15*, 61–76.
(4) Faller, P.; Hureau, C. *Dalton Trans.* **2009**, 1080–1094.
(5) Sayre, L. M.; Perry, G.; Atwood, C. S.; Smith, M. A. *Cell. Mol. Biol. (Oxford)* **2000**, *46*, 731.
(6) Gomez-Balderas, R.; Raffa, D. F.; Rickard, G. A.; Brunelle, P.; Rauk, A. *J. Phys. Chem. A* **2005**, *109*, 5498.
(7) Raffa, D. F.; Gomez-Balderas, R.; Brunelle, P.; Rickard, G. A.; Rauk, A. *J. Biol. Inorg. Chem.* **2005**, *10*, 887.
(8) Raffa, D. F.; Rauk, A. *J. Phys. Chem. B* **2007**, *111*, 3789.
(9) Hewitt, N.; Rauk, A. *J. Phys. Chem. B* **2009**, *113*, 1202.
(10) Zirah, S.; Kozin, S. A.; Mazur, A. K.; Blond, A.; Cheminant, M.; Segalas-Milazzo, I.; Debey, P.; Rebuffat, S. *J. Biol. Chem.* **2006**, *281*, 2151–2161.
(11) Lovell, M. A.; Robertson, J. D.; Teesdale, W. J.; Campbell, J. L.; Markesbery, W. R. *J. Neurol. Sci.* **1998**, *158*, 47.
(12) Miura, T.; Suzuki, K.; Takeuchi, H. *J. Mol. Struct.* **2001**, *598*, 79.
(13) Miura, T.; Suzuki, K.; Kohata, N.; Takeuchi, H. *Biochemistry* **2000**, *39*, 7024.
(14) Nakamura, M.; Shishido, N.; Nunomura, A.; Smith, M. A.; Perry, G.; Hayashi, Y.; Nakayama, K.; Hayashi, T. *Biochemistry* **2007**, *46*, 12737–12743.
(15) Jiang, D. L.; Li, X. J.; Williams, R.; Patel, S.; Men, L. J.; Wang, Y. S.; Zhou, F. M. *Biochemistry* **2009**, *48*, 7939.
(16) Frisch, M. J.; Trucks, G. W.; Schlegel, H. B.; Scuseria, G. E.; Robb, M. A.; Cheeseman, J. R.; Montgomery, J. A., Jr.; Vreven, T.; Kudin, K. N.; Burant, J. C.; Millam, J. M.; Iyengar, S. S.; Tomasi, J.; Barone, V.; Mennucci, B.; Cossi, M.; Scalmani, G.; Rega, N.; Petersson, G. A.;

Nakatsuji, H.; Hada, M.; Ehara, M.; Toyota, K.; Fukuda, R.; Hasegawa, J.; Ishida, M.; Nakajima, T.; Honda, Y.; Kitao, O.; Nakai, H.; Klene, M.; Li, X.; Knox, J. E.; Hratchian, H. P.; Cross, J. B.; Adamo, C.; Jaramillo, J.; Gomperts, R.; Stratmann, R. E.; Yazyev, O.; Austin, A. J.; Cammi, R.; Pomelli, C.; Ochterski, J. W.; Ayala, P. Y.; Morokuma, K.; Voth, G. A.; Salvador, P.; Dannenberg, J. J.; Zakrzewski, V. G.; Dapprich, S.; Daniels, A. D.; Strain, M. C.; Farkas, O.; Malick, D. K.; Rabuck, A. D.; Raghavachari, K.; Foresman, J. B.; Ortiz, J. V.; Cui, Q.; Baboul, A. G.; Clifford, S.; Cioslowski, J.; Stefanov, B. B.; Liu, G.; Liashenko, A.; Piskorz, P.; Komaromi, I.; Martin, R. L.; Fox, D. J.; Keith, T.; Al-Laham, M. A.; Peng, C. Y.; Nanayakkara, A.; Challacombe, M.; Gill, P. M. W.; Johnson, B.; Chen, W.; Wong, M. W.; Gonzalez, C.; Pople, J. A. *Gaussian 03*, revision E.01; Gaussian Inc.: Wallingford, CT, 2004.

(17) Frisch, M. J.; Trucks, G. W.; Schlegel, H. B.; Scuseria, G. E.; Robb, M. A.; Cheeseman, J. R.; Scalmani, G.; Barone, V.; Mennucci, B.; Petersson, G. A.; Nakatsuji, H.; Caricato, M.; Li, X.; Hratchian, H. P.; Izmaylov, A. F.; Bloino, J.; Zheng, G.; Sonnenberg, J. L.; Hada, M.; Ehara, M.; Toyota, K.; Fukuda, R.; Hasegawa, J.; Ishida, M.; Nakajima, T.; Honda, Y.; Kitao, O.; Nakai, H.; Vreven, T.; Montgomery, J. A., Jr.; Peralta, J. E.; Ogliaro, F.; Bearpark, M.; Heyd, J. J.; Brothers, E.; Kudin, K. N.; Staroverov, V. N.; Kobayashi, R.; Normand, J.; Raghavachari, K.; Rendell, A.; Burant, J. C.; Iyengar, S. S.; Tomasi, J.; Cossi, M.; Rega, N.; Millam, N. J.; Klene, M.; Knox, J. E.; Cross, J. B.; Bakken, V.; Adamo, C.; Jaramillo, J.; Gomperts, R. E.; Stratmann, O.; Yazyev, A. J.; Austin, R.; Cammi, C.; Pomelli, J. W.; Ochterski, R.; Martin, R. L.; Morokuma, K.; Zakrzewski, V. G.; Voth, G. A.; Salvador, P.; Dannenberg, J. J.; Dapprich, S.; Daniels, A. D.; Farkas, O.; Foresman, J. B.; Ortiz, J. V.; Cioslowski, J.; Fox, D. J. *Gaussian 09*, revision A.02; Gaussian, Inc.: Wallingford, CT, 2009.

(18) Becke, A. D. *J. Chem. Phys.* **1993**, *98*, 5648–5652.

(19) Lee, C.; Yang, W.; Parr, R. G. *Phys. Rev. B* **1988**, *37*, 785–789.

(20) Stephens, P. J.; Devlin, F. J.; Chabalowski, C. F.; Frisch, M. J. *J. Phys. Chem.* **1994**, *98*, 11623–11627.

(21) Scott, A. P.; Radom, L. *J. Phys. Chem.* **1996**, *100*, 16502.

(22) Guthrie, J. P. *J. Phys. Chem. A* **2001**, *105*, 8495.

(23) Liao, M.-S.; Watts, J. D.; Huang, M.-J. *J. Comput. Chem.* **2006**, *27*, 1577.

(24) Cances, E.; Mennucci, B.; Tomasi, J. *J. Chem. Phys.* **1997**, *107*, 3032.

(25) Barone, V.; Cossi, M.; Tomasi, J. *J. Chem. Phys.* **1997**, *107*, 3210.

(26) Calculated as the difference between $\Delta_f G_{(g)}(H_2O)$ and $\Delta_f G_{(l)}(H_2O)$. The IEFPCM calculated value for water is $\Delta G_{solv}(H_2O)$ 30.3 kJ mol^{-1}.

(27) Tissandier, M. D.; Cowen, K. A.; Feng, W. Y.; Gundlach, E.; Cohen, M. H.; Earhart, A. D.; Coe, J. V.; Tuttle, T. R., Jr. *J. Phys. Chem. A* **1998**, *102*, 9308.

(28) 418 kJ mol^{-1} is the Gibbs free energy for the half-reaction, $^1/_2H_{2(g)} \rightarrow H_{(aq)}^+ + e^-$. It can be obtained by adding $\Delta_f G^\circ_{(g)}(H^+)$ = 1517 kJ mol^{-1}, $\Delta G_{solv}(H^+) = -1107$ kJ mol^{-1}, and the factor to change the $H_{(aq)}^+$ reference state to 1M, $-RT \ln(1/24.6)$ = 8 kJ mol^{-1}. Additionally, $\Delta_f G^\circ_{(g)}(H^+)$ = 1517 kJ mol^{-1} is computed from $\Delta_f G^\circ_{(g)}$-(H) = 203 kJ mol^{-1} plus $\Delta_f G^\circ_{(g)}(H^+ + e^-)$ = 1314 kJ mol^{-1}.

(29) Wondimagegn, T.; Rauk, A. *J. Phys. Chem. B* **2011**, *115*, 569.

(30) Rickard, G. A.; Gomez-Balderas, R.; Brunelle, P.; Raffa, D. F.; Rauk, A. *J. Phys. Chem. A* **2005**, *109*, 8361.

(31) Benn, M. H.; Rauk, A.; Swaddle, T. To be published.

(32) Hatcher, L. Q.; Hong, L.; Bush, W. D.; Carducci, T.; Simon, J. D. *J. Phys. Chem. B* **2008**, *112*, 8160.

(33) Atwood, C. S.; Scarpa, R. C.; Huang, X.; Moir, R. D.; Jones, W. D.; Fairlie, D. P.; Tanzi, R. E.; Bush, A. I. *J. Neurochem.* **2000**, *75*, 1219.

(34) Bard, A. J.; Faulkner, L. R. *Electrochemical Methods. Fundamentals and Applications*; John Wiley and Sons: New York, 2001.